Ceramics-Silikáty 63 (3), 261-266 (2019)
www.ceramics-silikaty.cz doi: 10.13168/cs.2019.0019

STRUCTURE CHARACTERIZATION AND ENERGY STORAGE EVALUATION OF MANGANESE-DOPED 0.7NBT–0.26ST–0.04BT CERAMICS

#ZONGYANG SHEN, YUANYING YU, DONGXU LI, FUSHENG SONG, WENQIN LUO, ZHUMEI WANG, YUEMING LI

Energy Storage and Conversion Ceramic Materials Engineering Laboratory of Jiangxi Province, China National Light Industry Key Laboratory of Functional Ceramic Materials, School of Materials Science and Engineering, Jingdezhen Ceramic Institute, Jingdezhen 333403, China

#E-mail: shenzongyang@163.com

Submitted April 10, 2019; accepted May 3, 2019

Keywords: Energy storage ceramics, Bismuth sodium titanate, Barium strontium titanate, Capacitor

0.7($Na_{0.5}Bi_{0.5}$)TiO_3–0.26$SrTiO_3$-0.04$BaTiO_3$ (0.7NBT–0.26ST–0.04BT) ceramics was chosen as the base material, and x mol. % $MnCO_3$ (x = 0, 0.1, 0.3, 0.5, 0.7) was externally introduced to investigate its effect on the phase structure, microstructure, dielectric and ferroelectric properties for energy storage. X-ray diffraction (XRD) analysis revealed that no diffraction peak location shifting but intensity weakening can be observed with manganese doping amount, indicating manganese did not enter the crystal lattice but form glass phases and/or impurities. Scanning electron microscopy (SEM) analysis showed that manganese doping promoted grain growth, and some liquid or precipitated impurity particles were found at grain boundaries, which was consistent with the results of XRD. Manganese doping can effectively suppress the dielectric loss near room temperature of the ceramics. When the doping amount of $MnCO_3$ was 0.5 mol. % and the applied electric field was only 60 kV·cm^{-1}, the optimal recoverable energy density and efficiency of the ceramics were 0.63 J·cm^{-3} and 65 % respectively, presenting a valuable solid state energy storage ceramic capacitor material.

INTRODUCTION

With the rapid development of electronic devices towards miniaturization, light weight and integration, it is urgent to find capacitor materials with high recoverable energy storage density [1, 2]. Basically, the recoverable energy storage density of dielectric material per unit volume γ can be evaluated by the integral formula (1) according to the polarization-electric field hysteresis (*P-E*) loops.

$$\gamma = \int_{P_s}^{P_r} E \, dP \quad (1)$$

in which E is the applied field, P is the polarization, P_s is the saturated polarization (normally alternative to maximum polarization P_{max}), and P_r is the remnant polarization [3, 4]. Therefore, dielectric materials with high P_r and the great difference between P_s and P_r will be prospective for high energy density storage applications [5].

Ferroelectric $Na_{0.5}Bi_{0.5}TiO_3$ (NBT), which presents a room temperature perovskite rhombohedral structure, having high Curie temperature (T_c = 320 °C) and large saturated polarization (P_s > 40 μC·cm^{-2}), but large remnant polarization (P_r = 38 μC·cm^{-2}) unsatisfied for energy storage applications. However, a so-called antiferroelectric (AFE)-like behavior due to an ergodic relaxor state at its depolarization temperature (T_d = 220 °C) can constrict the *P-E* loops, and then a lower P_r will be obtained [6,7]. Accordingly, it is desirable to shift the T_d down and then achieve an AFE-like behavior near room temperature in NBT meeting energy storage requirements [8]. Strontium titanate ($SrTiO_3$, ST) is an ideal cubic perovskite structure at room temperature and experiences a cubic to tetragonal phase transition when the temperature drops to 110 K [9], which has been extensively studied to shift the T_d downward to room temperature and then lower the remnant polarization P_r of NBT [10, 11]. Meanwhile, barium titanate ($BaTiO_3$, BT) was reported to form unlimited solid solution with ST to have tunable dielectric properties [12, 13], as well as form morphotropic phase boundary (MPB) with NBT to enhance ferroelectric, piezoelectric and dielectric properties [14-16]. Actually, in our previous work, BT modified NBT-ST with a composition of 0.7NBT–0.26ST–0.04BT was found to possess an optimized energy storage density and efficiency [17].

On the other hand, manganese has been widely reported to improve ferroelectric, piezoelectric and/or dielectric properties of functional ceramics, regardless of the introduction form of manganese dioxide, manganese carbonate or manganese nitrate, whether or not manganese enters the lattice in a stoichiometric ratio or remains at the grain boundary in an external form [18-21]. Therefore, in this work, we choose 0.7NBT–0.26ST–0.04BT as the base material, while manganese carbonate ($MnCO_3$) is introduced with the purpose of modifying the microstructure and *P-E* behavior of the ceramics, thereby improving the energy storage characteristics.

EXPERIMENTAL

Raw materials of 99.8 % Na_2CO_3, 99 % Bi_2O_3, 99 % $SrCO_3$, 99 % $BaCO_3$, 98 % TiO_2, and 99 % $MnCO_3$ from Sinopharm Chemical Reagent Co. Ltd., Shanghai, China were combined in our system $0.7(Na_{0.5}Bi_{0.5})TiO_3$–$0.26SrTiO_3$–$0.04BaTiO_3$ (0.7NBT–0.26ST–0.04BT) + + x mol. % $MnCO_3$ (x = 0, 0.1, 0.3, 0.5, 0.7) to prepare ceramic samples. The raw materials were weighed for each composition and ground for 24 h in zirconia ball mill at a speed of 120 rpm using ethanol medium. The mixture raw materials were calcined at 900 °C for 3 h and then ground again for 24 h. After drying, the calcined powders were added to the polyvinyl alcohol solution (PVA, 5 wt. %) as a binder for granulation. Disks (13 mm in diameter by 1 mm thick) were formed by pressing at 120 ± 10 MPa and first preheating for 2 h at 650 °C to remove organic binders, and then sintering for 3 h between 1100 °C and 1200 °C in an ambient atmosphere with a heating rate of 5 °C·min^{-1}.

X-ray diffraction (XRD, D8-Advance) analysis using CuK_α radiation was carried to determine the phase structure of polished sintered ceramic samples. Data analysis was carried out by Rietveld refinement using GSAS program suite. The microstructural characteristics of polished and thermally etched surface of sintered ceramics were observed by field emission scanning electron microscope (FE-SEM, JSM-5610LV). For dielectric measurements, the specimens were polished to about 0.6 mm thick, and then painted with silver pastes on both sides firing for 20 min at 800 °C to form electrodes. Weak-field dielectric constant and loss at 1 kHz as a function of temperature from room temperature to 500 °C were measured by a precision impedance analyzer (HP4294A, Agilent), joining a controlled-temperature cell. Room temperature polarization-electric field (*P-E*) loops were observed on a radiant precision workstation (TRek model 609B) using standard Sawyer and Tower circuits. The loops were obtained by applying 10 Hz ac with a 60 kV·cm^{-1} electric field to the specimens. By integrating the area between discharge curve and polarization axis of the *P-E* loop, the recoverable energy density and efficiency of the ceramic samples were evaluated.

RESULTS AND DISCUSSION

The XRD patterns of 0.7NBT-0.26ST-0.04BT ceramics with different manganese doping amount are shown in Figure 1a and b. It can be seen from Figure 1a that all samples are indexed a tetragonal perovskite main crystalline phase, and impurities are detected for the sample with x = 0.7 as marked by asterisks. Meanwhile, as seen from the enlarged (200)/(202) diffraction peaks shown in Figure 1b, no diffraction peak location shifting but gradually intensity weakening are observed for the ceramic samples with the increase of x value, indicating that doped manganese does not enter the crystal lattice but forms a liquid glass phase. Figure 1c shows the Rietveld refinement profile of pure 0.7NBT–0.26ST–0.04BT ceramics. The best fitting between observed and calculated intensities are obtained with space group of P4bm in the tetragonal symmetry, and the lattice parameters are of a = b = 0.55284 nm and c = 0.39104 nm.

Figure 2 gives the SEM micrographs of 0.7NBT–0.26ST–0.04BT ceramics with different manganese doping amount. For pure 0.7NBT-0.26ST-0.04BT ceramics (x = 0), as shown in Figure 2a, small and uniform grains with the size of 1-3 μm are observed. However, after manganese doping (see Figures 2b-d), the grain growth is promoted up to ~10 μm of size, which should be due to formation of liquid phase by manganese doping and then promoting grain growth. Furthermore, for the manganese doped ceramic samples (see Figures 2b-d), some small impurity particles can be seen on the grain surfaces or grain boundaries, and the number of impurity particles increases with the increase of

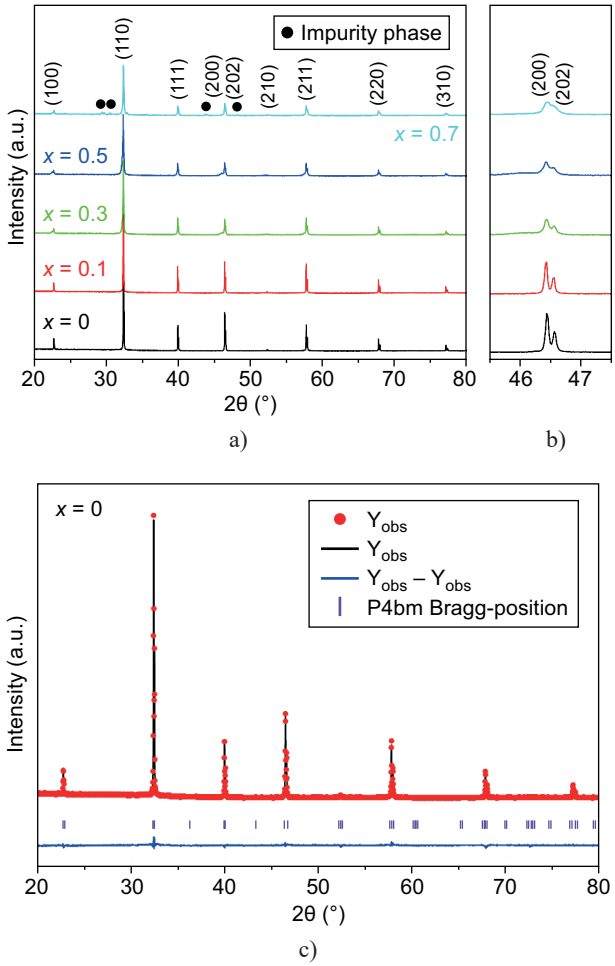

Figure 1. XRD patterns of 0.7NBT–0.26ST–0.04BT + x mol. % $MnCO_3$ ceramics in 2θ ranges of: a) 20 to 80°, and b) 45.5 to 47.5° (Figure 1c shows the Rietveld refinement profile of pure 0.7NBT–0.26ST–0.04BT ceramics).

manganese doping amount. This is basically consistent with the results of XRD analysis in Figure 1. However, it should be noted that the presence of impurities is not detected in XRD analysis when $x \leq 0.5$, which may be due to the fact that the content of impurities is low and does not reach the detection accuracy range of XRD technique.

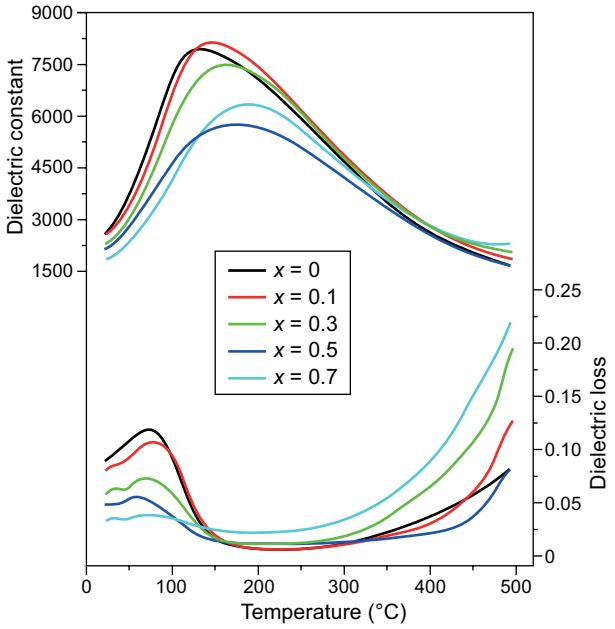

Figure 3. Temperature dependent dielectric constant and loss of 0.7NBT–0.26ST–0.04BT + x mol. % $MnCO_3$ ceramics (measurement was performed at 1 kHz upon heating process).

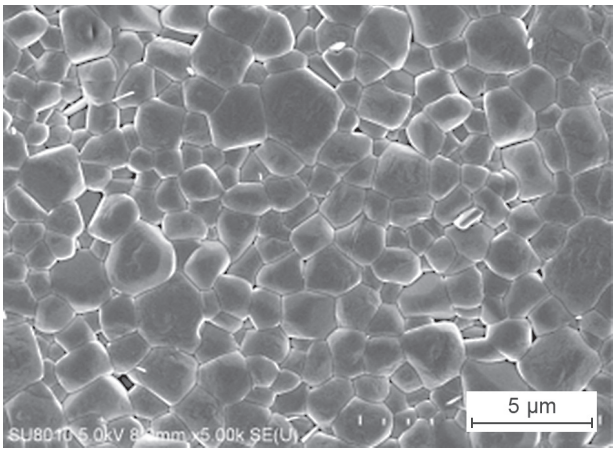

a) $x = 0$

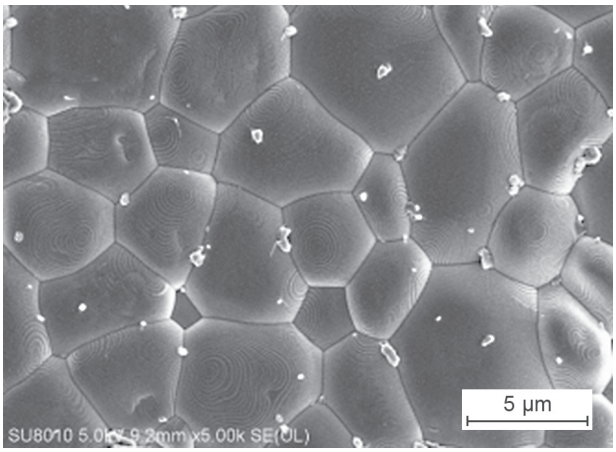

b) $x = 0.1$

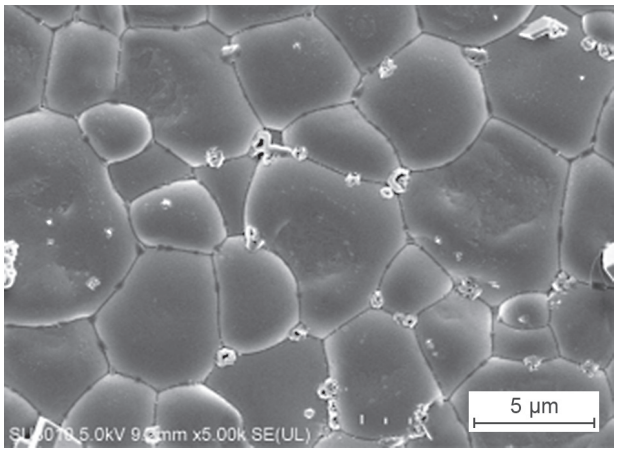

d) $x = 0.5$

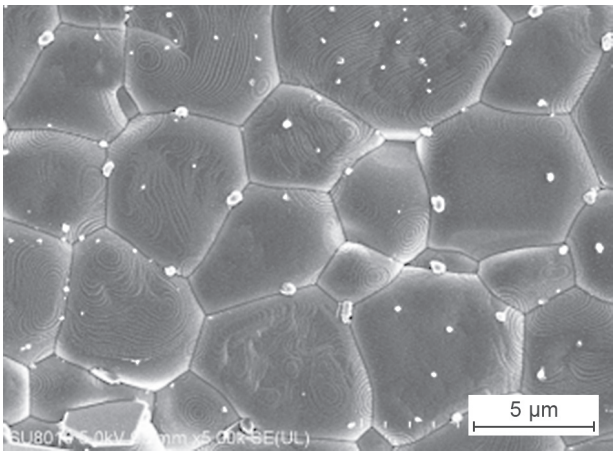

c) $x = 0.3$

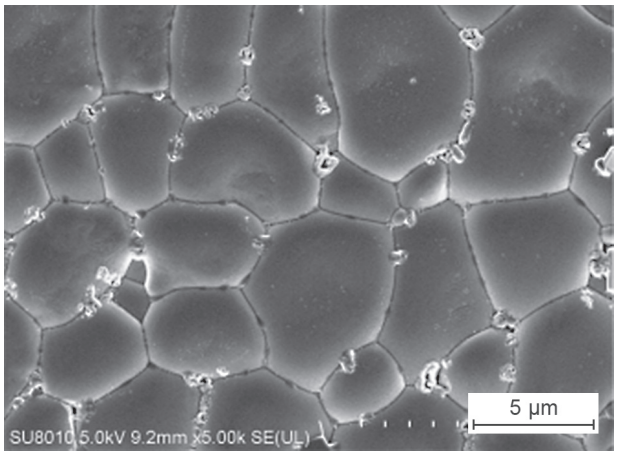

e) $x = 0.7$

Figure 2. SEM micrographs of the polished and thermally etched surface of 0.7NBT–0.26ST–0.04BT + x mol. % $MnCO_3$ ceramics: a) $x = 0$; b) $x = 0.1$; c) $x = 0.3$; d) $x = 0.5$; and e) $x = 0.7$.

The dielectric constant and loss as a function of temperature for 0.7NBT-0.26ST-0.04BT ceramics with different manganese doping amount are shown in Figure 3. T_m is assigned to a temperature at which the dielectric constant reaches a maximum value [22, 23]. As seen from Figure 3, the T_m gradually in-creases a little with increasing x value, which may be related to the increase of impurities induced by increasing manganese doping amount as observed in Figure 2. In particular, the inflection point in the dielectric loss curve around room temperature can be gradually suppressed with increasing x value, and even flattened when $x = 0.7$. This phenomenon should be related to the pinning effect caused by glass and/or impurity phases at grain boundaries, since both analysis of XRD in Figure 1 and SEM in Figure 2 indicate the presence of glass and/or impurity phases.

Figure 4 gives *P-E* loops of 0.7NBT–0.26ST–0.04BT ceramics with different manganese doping amount. With the increase of x value, the *P-E* hysteresis loops become more slanted and slim, accompanying with a gradually decrease of maximum polarization

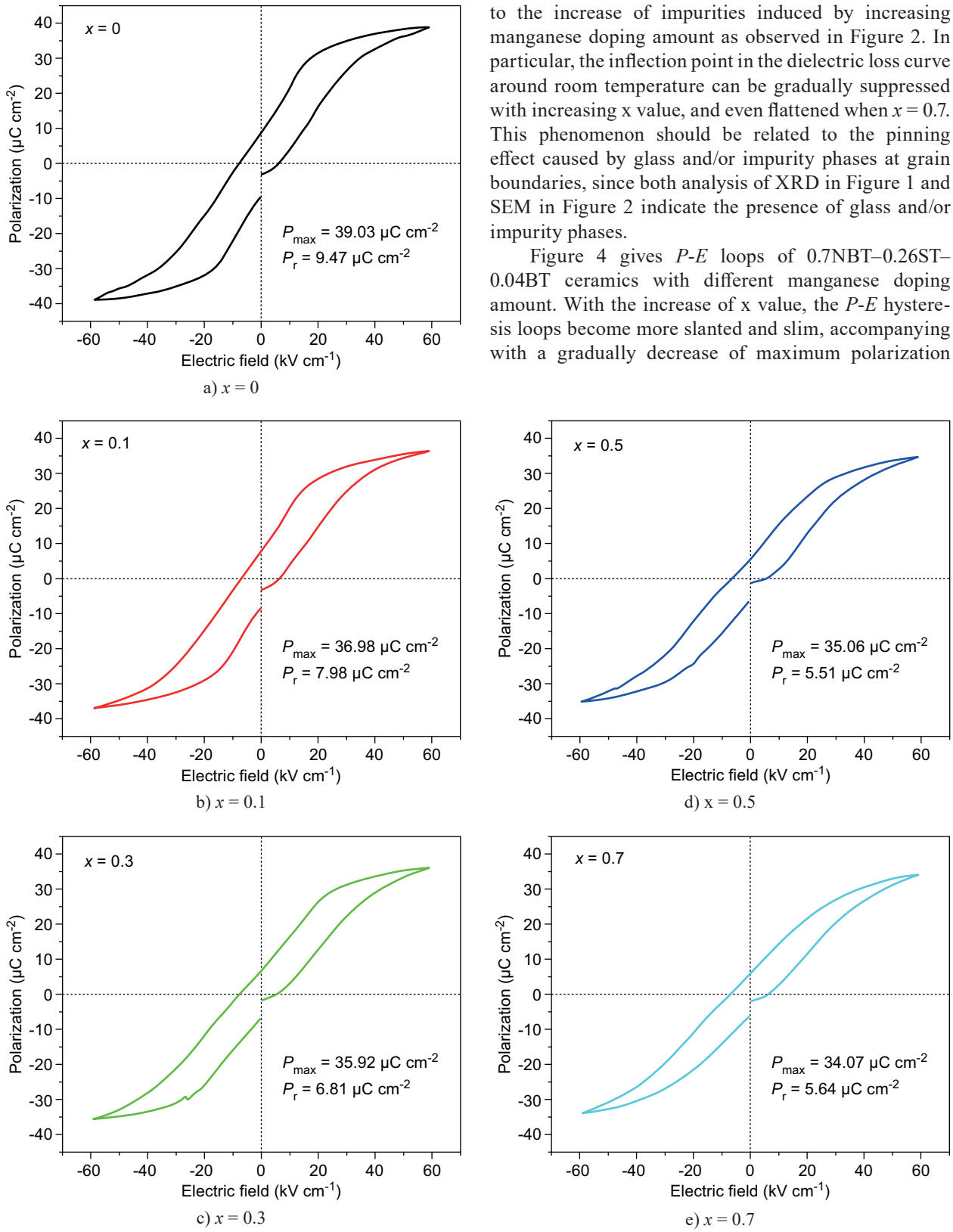

Figure 4. Polarization-electric field (*P-E*) hysteresis loops of 0.7NBT–0.26ST–0.04BT + x mol. % $MnCO_3$ ceramics: a) $x = 0$; b) $x = 0.1$; c) $x = 0.3$; d) $x = 0.5$; and e) $x = 0.7$.

(P_{max}) and a minimum remnant polarization (P_r = = 5.51 μC cm^{-2}) when x = 0.5. This is mainly due to the ferroelectric dilution of impurities and the pinning effect of grain boundary glass to main crystalline ferroelectric phase [24, 25].

Figure 5 gives the calculated recoverable energy density and efficiency according to *P-E* hysteresis loops in Figure 4. The highest recoverable energy density (γ = 0.63 J cm^{-3}) and efficiency (η = 65 %) are obtained for the ceramics with x = 0.5, which should be related to its slanted and slim *P-E* hysteresis loop with a relatively high P_{max} and a minimum P_r shown in Figure 4. This ceramic should be a promising material for solid state compact pulsed power capacitors.

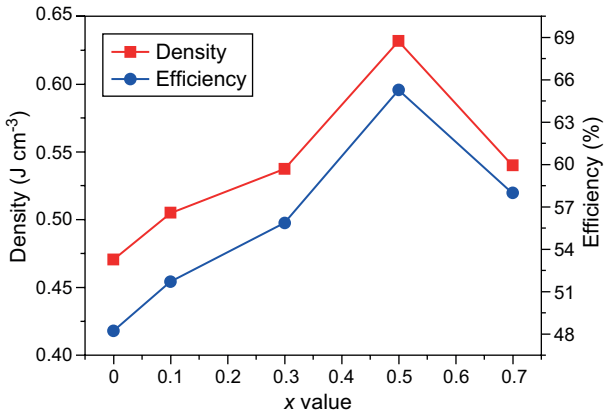

Figure 5. Recoverable energy storage density and efficiency of 0.7NBT–0.26ST–0.04BT ceramics as a function of manganese doping amount x value.

CONCLUSIONS

In summary, $MnCO_3$ was introduced to modify the structure and dielectric energy storage properties of 0.7NBT–0.26ST–0.04BT ceramics. The doped manganese should not enter the crystal lattice but forms a liquid glass phase and impurities, then dilute or suppress the dielectric and ferroelectric properties of the ceramics. For 0.7NBT–0.26ST–0.04BT ceramics doping with 0.5 mol. % $MnCO_3$, a slanted and slim *P-E* hysteresis loop with a relatively high P_{max} and a minimum P_r is obtained, leading to an optimized recoverable energy storage density (γ = 0.63 J·cm^{-3}) and efficiency (η = 65 %) beneficial for solid state power capacitor applications.

Acknowledgments

This work was financially supported by National Natural Science Foundation of China (51767010) and Science & Technology Key Research Project of Jiangxi Provincial Education Department (GJJ170760).

REFERENCES

1. Yao Z., Song Z., Hao H., Yu Z., Cao M., Zhang S., Lanagan M. T., Liu H. (2017): Homogeneous/Inhomogeneous-Structured Dielectrics and their Energy-Storage Performances. Advanced Materials, 29, 1601727. Doi: 10.1002/adma.201601727
2. Zhao L., Liu Q., Gao J., Zhang S., Li J.F. (2017): Lead-Free Antiferroelectric Silver Niobate Tantalate with High Energy Storage Performance. Advanced Materials, 29, 1701824. Doi: 10.1002/adma.201701824
3. Hao X. (2013): A review on the dielectric materials for high energy-storage application. Journal of Advanced Dielectrics, 3, 1330001. Doi: 10.1142/S2010135X13300016
4. Burn I., Smyth D. M. (1972): Energy Storage in Ceramic Dielectrics. Journal of Materials Science, 7, 339-343. Doi: 10.1007/BF00555636
5. Cao W., Li W., Zhang T., Sheng J., Hou Y., Feng Y., Yu Y., Fei W. (2015): High-Energy Storage Density and Efficiency of (1-x)[0.94NBT-0.06BT]-xST Lead-Free Ceramics. Energy Technology, 3, 1198-1204. Doi: 10.1002/ente.201500173
6. Smolenskii G. A., Isupov V. A., Agranovskaya A. I., Krainik N. N. (1961): New Ferroelectrics of Complex Composition IV. Sov. Physics Solid State, 2, 2651-2654.
7. Tu C. S., Siny I. G., Schmidt V. H. (1994): Sequence of Dielectric Anomalies and High-Temperature Relaxation Behavior in $Na_{1/2}Bi_{1/2}TiO_3$. Physical review B, 49, 11550-11559. Doi: 10.1103/PhysRevB.49.11550
8. Liu X., Shi J., Zhu F., Du H., Li T., Liu X., Lu H. (2018): Ultrahigh energy density and improved discharged efficiency in bismuth sodium titanate based relaxor ferroelectrics with A-site vacancy. Journal of Materiomics, 4, 202-207. Doi: 10.1016/j.jmat.2018.05.006
9. Muller K. A., Burkard H. (1979): $SrTiO_3$: An intrinsic quantum paraelectric below 4 K. Physical review B, 19, 3593. Doi: 10.1103/PhysRevB.19.3593
10. Hiruma Y., Imai Y., Watanabe Y., Nagata H., Takenaka T. (2008): Large electrostrain near the phase transition temperature of $Bi_{0.5}Na_{0.5}TiO_3$–$SrTiO_3$ ferroelectric ceramics. Applied Physics Letters, 92, 262904. Doi: 10.1063/1.2955533
11. Malathi A. R., Devi Ch. S., Kumar G. S., Vithal M., Prasad G. (2013): Dielectric relaxation in NBT-ST ceramic composite materials. Ionics, 19, 1751. Doi: 10.1007/s11581-013-0921-2
12. Wang Y., Shen Z. Y., Li Y., Wang Z., Luo W. Q., Hong Y. (2015): Optimization of energy storage density and efficiency in $Ba_xSr_{1-x}TiO_3$ (x≤0.4) paraelectric ceramics. Ceramics International, 41, 8252-8256. Doi: 10.1016/j.ceramint.2015.02.156
13. Alexandru H. V., Berbecaru C., Loachim A., Nedelcu L., Dutu A. (2006): BST solid solutions, temperature evolution of the ferroelectric transitions. Applied Surface Science, 253, 354-357. Doi: 10.1016/j.apsusc.2006.06.011
14. Damjanovic D., Klein N., Li J., Porokhonskyy V. (2010): What can be expected from lead-free piezoelectric materials? Functional Materials Letters, 3, 5-13. Doi: 10.1142/S1793604710000919
15. McQuade R. R., Dolgos M. R. (2016): A review of the structure-property relationships in lead-free piezoelectric (1-x)$Na_{0.5}Bi_{0.5}TiO_3$-(x)$BaTiO_3$. Journal of Solid State Chemistry, 242, 140-147. Doi: 10.1016/j.jssc.2016.01.008

16. Duan R., Wang J., Jiang S., Lv Y., Li J., Song A., Liang L., Liu Y. (2018): Effect of some dopants on piezomodulus d_{33} of $0.94Na_{0.5}Bi_{0.5}TiO_3$-$0.06BaTiO_3$ lead-free relaxor ferroelectrics ceramics. Journal of Materials Science: Materials in Electronics, 29, 13952-13956.
17. Luo W. Q., Shen Z. Y., Yu Y., Song F., Wang Z., Li Y. (2018): Structure and dielectric properties of NBT-xBT-ST lead-free ceramics for energy storage. Journal of Advanced Dielectrics, 8, 1820004. Doi: 10.1142/S2010135X18200047
18. Chen L., Fan H., Zhang S. (2017): Investigation of MnO_2-doped (Ba, Ca)TiO_3 lead-free ceramics for high power piezoelectric applications. Journal of the American Ceramic Society, 100, 3568-3576. Doi: 10.1111/jace.14894|
19. Wang X., Liang P., Chao X., Yang Z. (2015): Dielectric Properties and Impedance Spectroscopy of $MnCO_3$-Modified $(Ba_{0.85}Ca_{0.15})(Zr_{0.1}Ti_{0.9})O_3$ Lead-Free Ceramics. Journal of the American Ceramic Society, 98, 1506-1514. Doi: 10.1111/jace.13481|
20. Sopyan I., Ramesh S., Nawawi N. A., Tampieri A., Sprio S. (2011): Effects of manganese doping on properties of sol-gel derived biphasic calcium phosphate ceramics. Ceramics International, 37, 3703-3715. Doi: 10.1016/j.ceramint.2011.06.033
21. Tang Y., Shen Z. Y., Zhao X., Wang F., Shi W., Sun D., Zhou Z., Zhang S. (2018): Pyroelectric properties of Mn-doped Aurivillius ceramics with different pseudo-perovskite layers. Journal of the American Ceramic Society, 101, 1592-1597. Doi: 10.1111/jace.15267|
22. Hiruma Y., Nagata H., Takenaka T. (2008): Phase diagrams and electrical properties of $(Bi_{1/2}Na_{1/2})TiO_3$-based solid solutions. Journal of Applied Physics, 104, 124106. Doi: 10.1063/1.3043588
23. Jo W., Schaab S., Sapper E., Schmitt L. A., Kleebe H. J., Bell A. J., Rödel J. (2011): On the phase identity and its thermal evolution of lead free $(Bi_{1/2}Na_{1/2})TiO_3$-6 mol% $BaTiO_3$. Journal of Applied Physics, 110, 074106. Doi: 10.1063/1.3645054
24. Shen Z. Y., Yu Y., Wang Y., Zhang L., Luo W. Q., Wang Z., Li Y. (2018): Reduced high temperature dielectric loss in BSB glass modified $Ba_{0.3}Sr_{0.7}TiO_3$ ceramics for energy storage. Journal of Materials Science: Materials in Electronics, 29, 1093-1097. Doi: 10.1007/s10854-017-8010-3
25. Yang H., Yan F., Lin Y., Wang T. (2018): Enhanced energy storage properties of $Ba_{0.4}Sr_{0.6}TiO_3$ lead-free ceramics with Bi_2O_3-B_2O_3-SiO_2 glass addition. Journal of the European Ceramic Society, 38, 1367-1373. Doi: 10.1016/j.jeurceramsoc.2017.11.058